Ultrasound in Med. & Biol., Vol. 00, No. 00, pp. 1–13, 2021

0301-5629/$ - see front matter

https://doi.org/10.1016/j.ultrasmedbio.2021.01.014

● *Original Contribution*

FOCUSED ULTRASOUND AND MICROBUBBLE TREATMENT INCREASES DELIVERY OF TRANSFERRIN RECEPTOR-TARGETING LIPOSOMES TO THE BRAIN

MARIEKE OLSMAN,* VIKTORIA SERETI,† MELINA MÜHLENPFORDT,* KASPER BENDIX JOHNSEN,† THOMAS LARS ANDRESEN,† ANDREW JAMES URQUHART,† and CATHARINA DE LANGE DAVIES*

* Department of Physics, Norwegian University of Science and Technology, Trondheim, Norway; and † Department of Health Technology, Technical University Denmark, Kongens Lyngby, Denmark

(*Received* 2 *October* 2020; *revised* 6 *January* 2021; *in final from* 13 *January* 2021)

Abstract—The blood-brain barrier (BBB) is a major obstacle to treating several brain disorders. Focused ultrasound (FUS) in combination with intravascular microbubbles increases BBB permeability by opening tight junctions, creating endothelial cell openings, improving endocytosis and increasing transcytosis. Here we investigated whether combining FUS and microbubbles with transferrin receptor-targeting liposomes would result in enhanced delivery to the brain of post-natal rats compared with liposomes lacking the BBB-targeting moiety. For all animals, increased BBB permeability was observed after FUS treatment. A 40% increase in accumulation of transferrin receptor-targeting liposomes was observed in the FUS-treated hemisphere, whereas the isotype immunoglobulin G liposomes showed no increased accumulation. Confocal laser scanning microscopy of brain sections revealed that both types of liposomes were mainly observed in endothelial cells in the FUS-treated hemisphere. The results demonstrate that FUS and microbubble treatment combined with BBB-targeting liposomes could be a promising approach to enhance drug delivery to the brain. (E-mail: marieke.olsman@ntnu.no)

Key Words: **Transferrin receptor-targeting, Blood–brain barrier disruption, Ultrasound, Liposomes, Microbubbles.**

INTRODUCTION

The blood-brain barrier (BBB) strictly controls the transport of substances into the brain, impeding the access of most drugs to the brain and preventing efficient treatment of many brain diseases (Abbott et al. 2010; Pardridge 2012). Several approaches for circumventing the BBB (*e.g.,* intranasal delivery, intracerebral/intraventricular injections, chemical mediation) have been proposed, but each of these approaches has several limitations, including low delivery efficiency, damage of healthy tissue and cytotoxic or adverse systemic effects (Rapoport 2000; Dhuria et al. 2010; White et al. 2011; Lochhead and Thorne 2012). To overcome these limitations, non-invasive approaches are highly needed for controlled transient and safe increase in BBB permeability to enable passage of large therapeutics into the brain.

Extensive research has been done on the use of focused ultrasound (FUS) in combination with intravascular microbubbles (MBs) for a transient and safe increase in BBB permeability (Hynynen et al. 2001; Meairs and Alonso 2007; McDannold et al., 2008a; McDannold et al., 2008b; Ting et al. 2012; Burgess and Hynynen 2013; Liu et al. 2014; Burgess et al. 2015; Poon et al. 2016). Successful delivery of chemotherapeutics, nanocarriers, antibodies and stem cells across the BBB after FUS-induced increase in BBB permeability have been reported (Liu et al. 2010; Burgess et al. 2011; Etame et al. 2012; Alkins et al. 2013; Åslund et al. 2015; Kobus et al. 2016; Poon et al. 2016). The exact mechanisms have still not been fully elucidated, but in the presence of ultrasound (US), MBs oscillate and apply biomechanical forces on the blood vessel wall, which potentially facilitate both trans- and paracellular transport across the capillary wall (Sheikov et al.

Address correspondence to: Marieke Olsman, Department of Physics, Norwegian University of Science and Technology, Høgskoleringen 5, 7491 Trondheim, Norway. E-mail: marieke.olsman@ntnu.no

2004; Alonso et al. 2010; Cho et al. 2011; Burgess and Hynynen 2013; Nhan et al. 2013). The resulting increased permeability of the BBB can lead to improved extravasation, distribution in the brain parenchyma and therapeutic efficacy of the drug (Liu et al. 2010; Treat et al. 2012).

To exploit the FUS-induced transport pathways to the fullest, a high concentration of the drug at the site of BBB disruption (BBBD) is favorable. This is often achieved by performing the happened by accident, no comments. FUS treatment directly after intravenous administration of the drug. Another approach is to use drug-loaded MBs, either with or without additional targeting to the BBB, which release the drug locally when sonicated (Ting et al. 2012; Fan et al. 2013, 2015, 2016). In the present study, we combined an FUS-induced increase in BBB permeability with intravenous administration of transferrin receptor (TfR)-targeting liposomes. The TfR has received special interest because its expression is restricted to the brain capillary endothelial cells (BCECs) compared with other endothelial cells (Jefferies et al. 1984). We hypothesize that this combined approach will improve the delivery of the drug nanocarrier across the BBB compared with a drug nanocarrier lacking the targeting moiety.

To study this, TfR-targeting and isotype immunoglobulin G (IgG) liposomes were loaded with cisplatin and labeled with a fluorophore. As a model system, postnatal rats were used because of their high TfR expression in the BBB (Taylor and Morgan 1990; Moos et al. 1998). Magnetic resonance imaging (MRI)-guided FUS was used to increase the permeability of the BBB, and the extent of permeability was evaluated by contrast-enhanced MRI. The amount of cisplatin (a model drug acting as a surrogate marker of the liposomes) entering the brain tissue was quantified by inductively coupled plasma mass spectrometry (ICP-MS). The distribution of liposomes in brain tissue was imaged by confocal laser scanning microscopy (CLSM).

MATERIALS AND METHODS

Materials

Ovine cholesterol, 1,2-distearoyl-*sn*-glycero-3-phosphocholine (DSPC), 2-distearoyl-*sn*-glycero-3-phosphoethanolamine-N-[methoxy(polyethylene glycol)-2000] (DSPE-PEG2000) and 1,2-distearoyl-*sn*-glycero-3-phosphoethanolamine-N-[maleimide(polyethylene glycol)-2000] (ammonium salt; DSPE-PEG2000-maleimide) were purchased from Avanti Polar Lipids, Inc. (Alabaster, USA); 1,1′-dioctadecyl-3,3,3′,3′-tetramethylindodicarbocyanine, 4-chlorobenzenesulfonate salt (DiD), 2-iminothiolane (Traut's reagent), the Micro BCA Protein Assay Kit and mouse IgG2a were from Thermo Fisher Scientific (Hvidovre, Denmark); phosphor, platinum, gallium and iridium elemental standards were from Fluka; and cisplatin (*cis*-diamminedichloroplatinum) and all other chemicals were from Sigma-Aldrich (Brøndby, Denmark). The mouse anti-rat TfR antibody (OX26) was a kind gift from Professor Torben Moos (Aalborg University, Denmark).

Table 1. Molar composition (%) of the liposomes

Lipid	Isotype IgG	Anti-TfR batch 1	Anti-TfR batch 2
DSPC	56.1	56.1	56.3
Chol	38.2	38.2	38.2
DSPE-PEG2000	5	5	5
DSPE-PEG2000-maleimide	0.5	0.5	0.5
DiD	0.2	0.2	—

DSPC=1,2-distearoyl-sn-glycero-3-phosphocholine; Chol = cholesterol; DSPE-PEG2000 = 2-distearoyl-*sn*-glycero-3-phosphoethanolamine-N-[methoxy(polyethylene glycol)-2000]; DSPE-PEG2000-maleimide = 1,2-distearoyl-*sn*-glycero-3-phosphoethanolamine-N-[maleimide(polyethylene glycol)-2000]; DiD = 1,1′-dioctadecyl-3,3,3′,3′-tetramethylindodicarbocyanine, 4-chlorobenzenesulfonate salt; IgG = immunoglobulin G; TfR = transferrin receptor.

Liposome formulation

The molar concentrations of the lipids used in the formulations are listed in Table 1. Lipids and DiD, in case of the fluorophore-labeled formulations, were dissolved in a mixture of *tert*-butanol and Milli-Q purified water (9:1), snap frozen in liquid nitrogen and freeze-dried overnight. The following day, an 8 mg/mL solution of cisplatin was heated to 70˚C and used to hydrate the thin lipid layers. During the hydration process the temperature was kept at 70˚C and the samples were under constant stirring. Next, the samples were extruded using a high-pressure extruder at 70˚C through a 100 nm filter to form small unilamellar vesicles. Thereafter, the formulations were dialyzed twice with phosphate-buffered saline (PBS) for 12 h each to remove un-encapsulated cisplatin.

Antibody thiolation

The liposomes were functionalized with an antibody against either the rat TfR (OX26) or an isotype IgG. The buffer of the antibodies was exchanged to 0.1 M borate and 2 mM dipotassium ethylenediaminetetraacetic acid (pH 8; K_2EDTA) by two rounds of spin filtration using Amicon Ultra-4 Centrifugal Filter Units (molecular-weight cutoff, 30 kDa; Sigma-Aldrich, Brøndby, Denmark) at 4000 *g* and 4˚C. Afterwards, the concentration of the antibody was measured using the absorbance at 280 nm of the solution using a NanoDrop 2000c spectrophotometer (Thermo Fisher Scientific, Hvidovre, Denmark) and the extinction coefficient of mouse IgGs (1.37). Traut's reagent was prepared by dissolving it in a borate buffer at a concentration of 2 mg/mL. OX26 or IgG antibodies and Traut's reagent

were mixed with a molar ratio of 1:40. The thiolation reaction was allowed to proceed for 1 h at room temperature under mild agitation. Afterward, the thiolated antibodies were purified from the residual Traut's reagent by spin filtration using Amicon Ultra-4 Centrifugal Filter Units (molecular-weight cutoff, 30 kDa) and PBS at 4000 *g* and 4˚C, twice.

Liposome preparation and purification

Liposomes containing DSPE-PEG2000-maleimide were mixed with thiolated OX26 or IgG antibodies at a molar ratio of 5:1 (as defined by available maleimide groups), the air phase of the container was replaced with N_2 and the antibodies were allowed to conjugate to the liposomes overnight in the dark under mild agitation. The following day, the liposomes were separated from unconjugated antibodies by size-exclusion chromatography, using a Sepharose CL-4B column (1.5 × 20 cm; Sigma-Aldrich, Brøndby, Denmark), PBS as an elution buffer and a flow rate of 1 mL/min. The absorbance at 280 nm of the resulting fractions was measured, and fractions with high absorbance were pooled and up-concentrated using Amicon Ultra-15 Centrifugal Filter Units (molecular-weight cutoff, 100 kDa) centrifuged at 4000 *g* and 4˚C. The fluorescence of the up-concentrated fractions was measured using a microplate reader (Spark, Tecan Trading, Männedorf, Switzerland) and used for pooling liposome-containing fractions.

Liposome characterization

The hydrodynamic radius, polydispersity index and zeta potential of the liposomes were measured using a Zetasizer ZS (Malvern Panalytical Ltd., Malvern, UK), by dilution in PBS for size and polydispersity index measurements and 4-(2-hydroxyethyl)-1-piperazineethanesulfonic acid (HEPES) 5% glucose buffer for zeta potential measurements. Phosphor and platinum concentrations were measured in the final liposome formulations using ICP-MS (see later). The Micro BCA Assay was used to confirm the presence of antibodies in final liposome samples, following the test tube manufacturer's protocol adjusted for microplate volumes.

Animals

Two pregnant Sprague Dawley rats were purchased (Janvier Labs, Le Genest-Saint-Isle, France) and housed separately in individually ventilated cages under conditions free of specific pathogens. Cages were kept in a controlled environment (20−23˚C; humidity, 50%−60%) on a 12 h night/day cycle and the animals had free access to food and sterile water. Housing, nesting material and gnaw sticks were used to enrich the cage. The study included 17 pups with a post-natal age of 14−17 days: 13 for ICP-MS analysis and 4 for confocal microscopy. All experimental procedures were approved by the Norwegian Food Safety Authority.

Magnetic resonance imaging

MRI was performed on a 7.05 T horizontal bore magnet (Biospec 70/20 Avance III, Bruker, Billerica, USA) with an 86 mm volume resonator for radio-frequency transmission and a phased-array rat-brain surface coil for reception.

Before, after and 24 h after BBBD, a T1 fast low-angle shot (FLASH) sequence was acquired to verify the increased BBB permeability by the detection of extravasated gadolinium-based MRI contrast agent (1 mL/kg, 0.5 mmol/mL, Omniscan; GE Healthcare, Chicago, USA), using the following acquisition properties: echo time (TE), 3.5 ms; repetition time (TR), 200 ms; flip angle, 40˚; 12 averages; slice thickness, 0.8 mm. A T2-weighted rapid acquisition with relaxation enhancement image was acquired to detect hemorrhages and edema, with the following acquisition properties: TE, 54 ms; TR, 2000 ms; 14 averages; slice thickness, 0.8 mm. All sequences had a field of view of 20 × 20 mm, with a matrix size of 200 × 200, and 12 slices spaced at 1 mm. MRI acquisition parameters were set using Bruker ParaVision 6.0.1.

BBBD treatment

The timeline of the experimental procedure is presented in Figure 1a. Animals were anesthetized using ∼2% isoflurane in medical air (78%) and oxygen (20%), after which they were cannulated in the lateral tail vein. The head was shaved with a hair trimmer and the remaining hair was removed with depilatory cream. Animals were randomly divided into two groups and received an injection of either Anti-TfR or isotype IgG liposomes (Anti-TfR batch 1 and isotype IgG: cisplatin 154 μg/kg; Anti-TfR batch 2, cisplatin 340 μg/kg). The liposomes were allowed to circulate for 1.5 h to give the Anti-TfR liposomes enough time to bind to the BCECs (Kucharz et al. 2020) before the animals were positioned in supine position on the MRI compatible animal bed, received a bolus injection of a gadolinium-based contrast agent and underwent a pre-BBBD MRI scan. During MRI imaging and US experiments, oxygen was excluded from the anesthesia mixture to extend the lifetime of the MBs (Mullin et al. 2011). Respiration rate was closely monitored using a pressure-sensitive probe (SA Instruments, Stony Brook, USA), and body temperature was maintained with a heater during MRI and a heating lamp during US experiments.

The FUS treatment was planned based on the pre-BBBD MRI scan. A 6 × 3 grid of treatment spots—with a spot diameter of 1.6 mm, corresponding to the -3 dB US beam width—was placed on the right hemisphere on

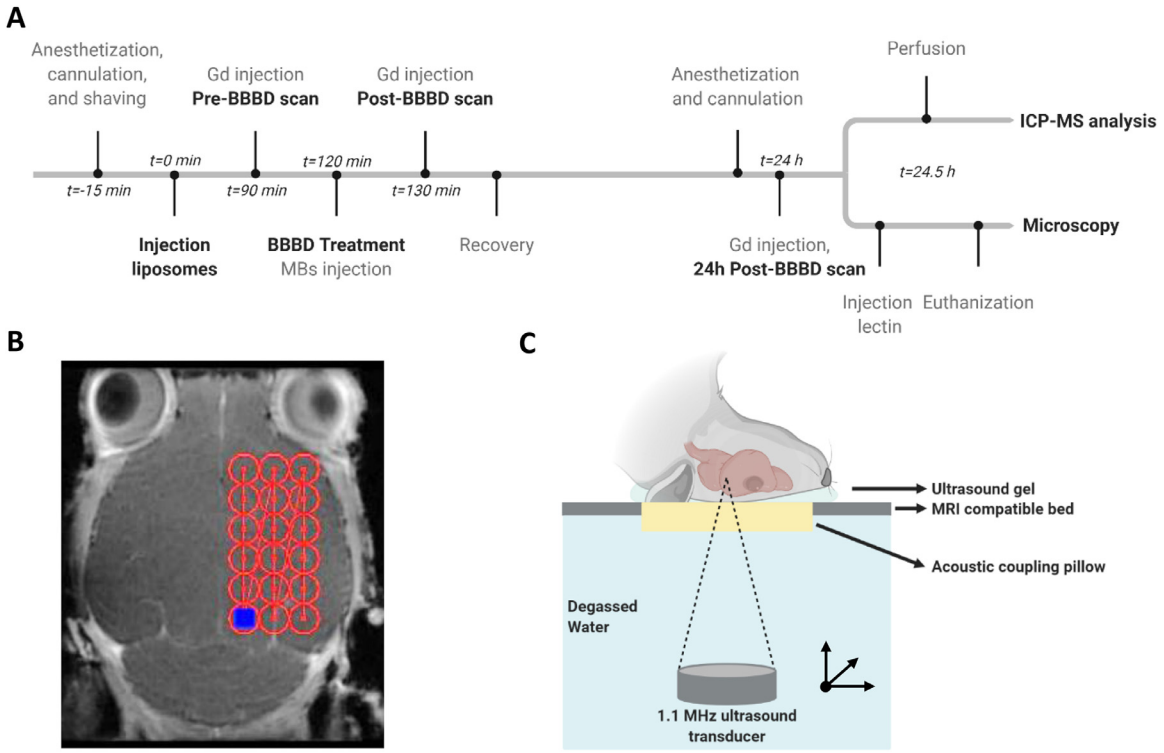

Fig. 1. Treatment timeline, planning and ultrasound setup. (a) Treatment timeline from anesthetization through treatment to ex vivo tissue analysis. (b) Treatment planning. The ultrasound beam scanned a 6 × 3 grid of spots (*red circle*) covering most of the right hemisphere. The blue spot indicates the current location of the ultrasound focus. (c) Ultrasound setup used for BBBD experiment. BBBD = blood-brain barrier disruption; Gd = gadolinium-based contrast agent; MB=microbubbles; ICP-MS=Inductively coupled plasma mass spectrometry; MRI=Magnetic resonance imaging.

an axial image at eye height in the rat's brain (Figure 1b). After the pre-BBBD MRI scan, the MRI bed with the animal was placed in the US setup (RK100, FUS Instruments, Toronto, Canada). The RK100 system consists of an arbitrary function generator, a 53 dB power amplifier, a 1.1 MHz US transducer with a focus at 60 mm and a computer with custom software for treatment planning. The experimental US setup is illustrated in Figure 1c. At 2 h after liposome injection, the animal received a bolus injection of SonoVue MBs (2 mL/kg; Bracco Imaging, Milan, Italy), and 10 s after the injection, the FUS treatment started.

The acoustic pressure was measured to be attenuated by the rat skull with approximately 27% ± 9% (see supplementary information p2), such that an *in situ* peak negative pressure of 0.22−0.29 MPa (corresponding to a mechanical index of 0.21−0.27) was obtained. A burst length of 10 000 cycles, repetition frequency of 0.25 Hz and total treatment time of 3 min were used. After FUS treatment, animals received another bolus injection of gadolinium-based contrast agent, and the MRI bed with the animal was placed back in the scanner and a post-BBBD scan was performed to detect BBBD, edema and hemorrhages.

After the post-BBBD MRI scan, the cannula was removed, the head was cleaned and the animal was taken off anesthesia and placed back in the cage with its dam and other pups. To study whether the permeability of the BBB was still increased at 24 h after BBBD, animals were anesthetized as already described and given an intravenous injection of gadolinium containing contrast agent before undergoing another MR scan (24 h post-BBBD). Thereafter, animals were euthanized with an intraperitoneal injection of pentobarbital (200 μL; concentration, 100 mg/mL) and kept under anesthesia until their breathing halted.

Animals used for measurement of the accumulation of liposomes in the brain by ICP-MS were transcardially perfused with PBS, after which the brain was excised. Animals whose brains were used for CLSM were injected with 50 μL of fluorescein-labeled *Lycopersicon esculentum* tomato lectin (2 mg/mL; Vector Laboratories, Peterborough, UK) to label functional blood vessels. The lectin was allowed to circulate for 5 min, after which the animal was euthanized and the brain excised. All samples were kept frozen until further analysis.

Analysis of BBBD

The degree of BBBD was evaluated by measuring the signal intensity in the T1 MR images using ImageJ (version 1.51j; USA). A square region of interest was drawn around six treatment spots and reused in four consecutive images all at eye height. Large brain structures were avoided. The same region of interest was used on the contralateral hemisphere (control). The ratio of the average intensity between the FUS-treated and control hemisphere was calculated to quantify the degree of BBBD. Visual examination of the T2 images was performed to assess hemorrhages (dark spots).

Inductively coupled plasma mass spectrometry

ICP-MS was used to quantify the amount of cisplatin found in the collected tissue samples. Tissue samples (maximum 100 mg) were digested in aqua regia overnight at 65˚C. Thereafter, samples were diluted in Milli-Q water containing 0.5 ppb iridium, followed by dilution in 2% hydrochloric acid containing 0.5 ppb iridium. Analysis was performed with an iCAP Q ICP-MS system (Thermo Fisher Scientific, Hvidovre, Denmark) fitted with an ASX-520 Autosampler and a ThermoFlex 2500 chiller. Before sample analysis, a TUNE B iCAP Q element mixture (Thermo Fisher Scientific, Hvidovre, Denmark) was used to calibrate the instrument. Serial dilution of an analytical standard platinum solution was used to generate a standard curve with data points in the 0.08−10 ppb range. In addition, the iridium content in each sample was measured as an internal standard. The same procedure was used to quantify the cisplatin content in the liposome formulations.

The phosphor content in the liposome formulation, which is an indicator of phospholipid concentration, was measured by diluting a sample of liposomes in 2% hydrochloric acid containing 0.5 ppb gallium. A standard curve with data points in the range of 25−100 ppm was generated based on serial dilution of an analytical standard phosphor solution.

Brain sectioning for CLSM

Excised brains were mounted transversely on a piece of cork with Tissue-Tek O.C.T. (Sakura, Alphen aan den Rijn, the Netherlands) before samples were submerged in liquid nitrogen.

Of the frozen brain samples, the first 1000 μm from the top was removed, after which three slices of 25 μm thick and two slices of 4 μm thick were taken. The latter two were stained with hematoxylin, erythrosine and saffron for histologic evaluation. This sectioning process was repeated every 900 μm until the whole brain was sectioned.

Confocal laser scanning microscopy

FUS-mediated delivery of the liposomes across the BBB was verified by imaging frozen brain sections with CLSM (LSM 800; Zeiss, Oberkochen, Germany). Before imaging, sections were thawed at room temperature and mounted with Vectashield (Vector Laboratories, Peterborough, UK). Tile scans of the whole brain section were acquired using a 20 × /0.8 Plan-Apochromat air objective lens (image properties: 512 × 512, 16 bit, pixel size 624 nm, 10% overlap between tiles). Lectin was excited with a 488 nm diode laser and emission was detected between 490 and 600 nm. The DiD was excited with a 640 nm laser diode and fluorescence was detected between and 700 nm. A 40 × /1.2 C-Apochromat water objective lens was used to obtain z-stacks of areas in both the FUS-treated and the untreated (control) hemisphere (image properties: 1024 × 1024, 16 bit, pixel size 156 nm, Airy scan, optical slice thickness 1.0 μm). A z-projection image (sum of slices) and 3-D rendering of the z-stack were acquired and used for presentation.

Statistical analysis

Statistical analysis on all data sets was performed with SigmaPlot (version 14.0; Systat Software Inc., San Jose, USA). Depending on the type and number of data sets compared, a paired *t*-test, unpaired *t*-test or one-way analysis of variance with Dunnett's multiple-comparison *post hoc* test was performed. The statistical test used will be specified in the caption of the corresponding figure. A *p* value smaller than 0.05 was considered to indicate statistical significance.

RESULTS

Increased BBB permeability after FUS treatment

FUS exposure in the presence of MBs resulted in a gadolinium-induced increase of the signal intensity, demonstrating that the BBB permeability was increased. Representative T1-weighted FLASH and corresponding T2 MR images before and after (10 min) FUS exposure are shown in Figure 2a. The observed intensity pattern of BBBD corresponded with the 6 × 3 grid of spots used during the FUS treatment and was observed along the coronal and sagittal planes of the brain (Supplementary Figure S1a). In all animals, the corresponding T2 images showed an increased signal intensity throughout the FUS-treated hemisphere (Supplementary Figure S1b), indicating the presence of edema. No clear spots representing hemorrhages were detected in either the T1 FLASH or T2 images, but the presence of hemorrhages could not be fully ruled out.

The extent of BBBD was evaluated based on the MR image intensity in the FUS-treated hemisphere relative to the control hemisphere (Fig. 2b). The permeability of the

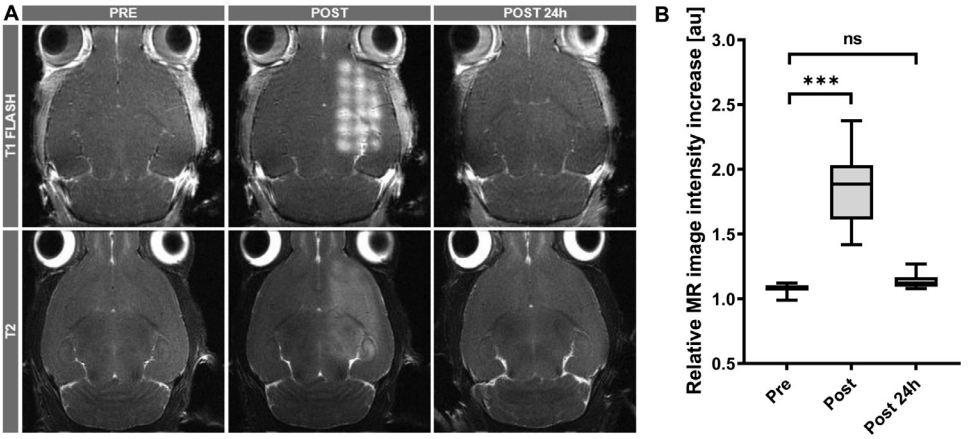

Fig. 2. (a) Representative T1 fast low-angle shot (FLASH) and T2 images of an animal pre, post and 24 h post focused ultrasound (FUS) treatment. Clear enhanced signal intensity is observed in the T1 FLASH and T2 images taken after FUS treatment, indicating successful disruption of the blood-brain barrier and the presence of edema, respectively. No clear hemorrhage spots can be observed in the T2 images. (b) Magnetic resonance image intensity increase in the FUS-treated hemisphere relative to the control hemisphere in the T1 FLASH images at the three time points. Asterisks show statistical significance (***$p < 0.001$, ns=not significant). The p values were derived from a one-way analysis of variance with Dunnett's multiple-comparison *post hoc* test, comparing the values of the post and post 24 h data sets to the pre-BBBD data set. Boxplot based on n = 17 animals.

BBB was successfully enhanced in all animals, but to different extents (Supplementary Figure S2). Between the animals treated with either the isotype IgG or the Anti-TfR liposomes, no difference in degree of BBBD was observed (Supplementary Figure S3). An increase in MR image intensity of approximately 1.7 times between the two hemispheres was observed in T1 images taken after FUS treatment, which was a statistically significant difference relative to the pre-BBBD scan. At 24 h after FUS treatment, the relative MR image-intensity increase had returned to pre-BBBD values.

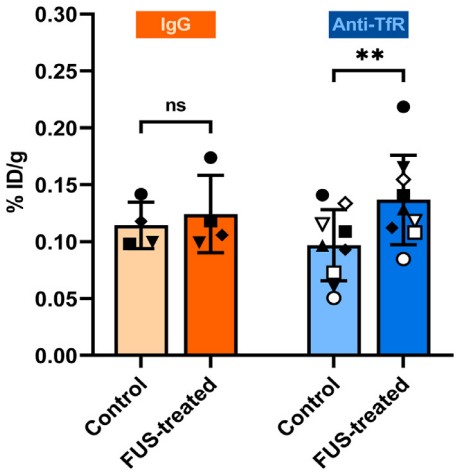

Fig. 3. Accumulation of cisplatin in the control and focused ultrasound (FUS)-treated hemispheres after injection with either the isotype immunoglobulin G (IgG) (*orange*) or the transferrin receptor-targeting liposome (Anti-TfR) (*blue*). Each symbol depicts an animal. In case of the Anti-TfR treatment group, black and white symbols indicate animals treated with batch 1 or batch 2 of the Anti-TfR liposome, respectively. The bar plot is presented as mean with standard deviations. Asterisks show statistical significance (**$p < 0.01$, ns=not significant). The p values are derived from a paired t-test; $n = 4$ and $n = 9$ for the isotype IgG and Anti-TfR treatment groups, respectively. %ID/g indicates percentage of injected dose per gram of tissue.

Increased accumulation of Anti-TfR liposomes in FUS-treated hemisphere measured by ICP-MS

FUS and MBs increased the accumulation of Anti-TfR liposomes by approximately 40%, whereas animals treated with the isotype IgG liposomes showed comparable accumulation in both hemispheres at 24 h after treatment (Figure 3). This time point was chosen to give the liposomes sufficient time to cross the BBB and diffuse into the brain parenchyma. Animals were perfused before tissue samples of each hemisphere were extracted, to remove cisplatin-loaded liposomes in circulation and avoid contamination of samples. Two batches of Anti-TfR liposomes were prepared, to have enough liposomes to inject the animals. The different formulations and batches showed similar liposomal characteristics (*e.g.,* diameter, Zeta potential; Table 2).

Liposomes in the FUS-treated hemisphere mainly observed in BCECs

Building upon the findings that FUS treatment increased the delivery of the Anti-TfR liposomes, a couple of brains from treated animals ($n = 2$ per liposome) were sectioned and imaged with CLSM to verify the presence of liposomes in the brain tissue. Sections from

Table 2. Characteristics of the cisplatin-loaded liposomes.

Liposome	Diameter, nm	Zeta potential, mV	PDI	CisPt concentration, mg/mL
Isotype IgG	178 ± 1.5	−11.7 ± 0.5	0.145 ± 0.02	0.054
Anti-TfR batch 1	180 ± 2.0	−10.6 ± 0.6	0.125 ± 0.01	0.054
Anti-TfR batch 2	181 ± 0.7	−13.5 ± 0.4	0.133 ± 0.018	0.093

PDI=polydispersity index; CisPt = cisplatin; IgG = immunoglobulin G; Anti-TfR = transferrin receptor-targeting.

different depths of the brain were imaged by CLSM and compared with the corresponding T1 FLASH MR images. In sections whose corresponding MR image showed clear gadolinium-enhanced contrast, the liposomes in the FUS-treated hemisphere seemed to be located in clusters (Figure 4a, 4e) corresponding to the grid of spots used during the FUS treatment (Figure 1b) and the gadolinium-enhanced contrast observed in the post-BBBD MRI scan (Figure 4d, 4h). Superimposing the liposome channel of the CLSM image with the corresponding MR image illustrated this more clearly (Supplementary Figure S4). Different extents of BBBD were observed at different levels of the brain. In MR images with low gadolinium-enhanced contrast, no clear pattern or increase in liposomal accumulation could be visually observed in the corresponding CLSM tile scan (Supplementary Fig. S5).

To determine whether the brain accumulation observed was owing to transport across the BBB and presence of the liposomes in the brain parenchyma, high-magnification CLSM was performed. In the control hemisphere, both liposomes were located in the blood vessels and no liposomes were observed in the brain parenchyma (Figure 5). In the FUS-treated hemisphere, both liposomes were observed either as diffusively staining BCECs or as a spotted structure aligned with the lectin staining. Representative CLSM images are shown in Figures 6 and 7 for animals treated with the isotype IgG and the Anti-TfR liposome, respectively. The corresponding 3-D renderings showed the location of the liposomes with respect to the lectin staining more clearly (Figsure 6b and 7b). In a few cases, a small number of

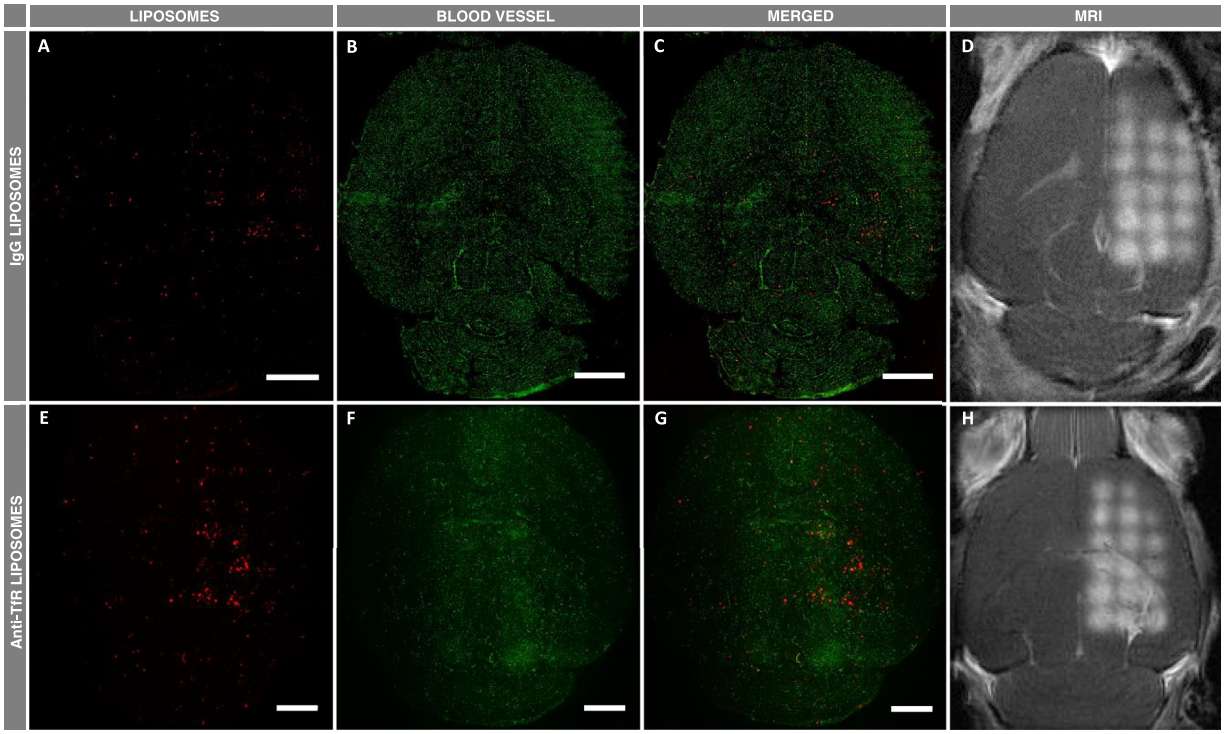

Fig. 4. Confocal laser scanning microscopy tile scans and corresponding magnetic resonance images of animals treated with the isotype immunoglobulin (IgG) (upper panel) and transferrin receptor-targeting (Anti-TfR) (lower panel) liposomes. (a, e) Liposomes (*red*) and (b, f) blood vessels (*green*) are shown separately and (c, g) merged. (d, h) Corresponding magnetic resonance images have been selected based on the brain structures observed in the tile scan. Scale bar is 2000 μm. MRI=magnetic resonance imaging.

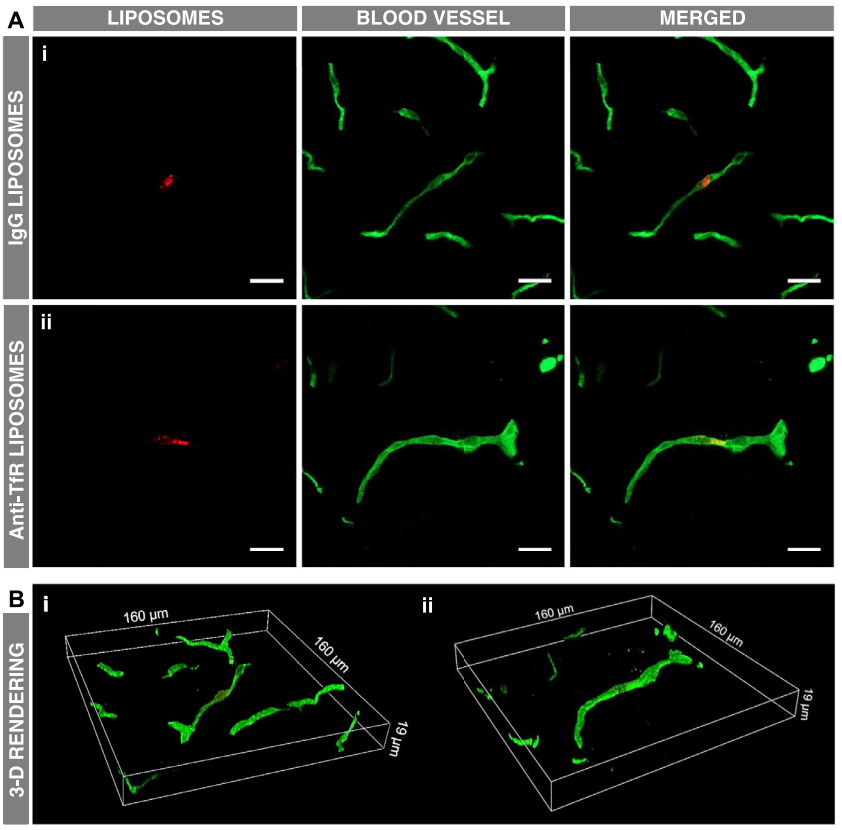

Fig. 5. (a) Representative confocal laser scanning microscopy images acquired in the control hemisphere of animals treated with the (i) isotype immunoglobulin G (IgG) and (ii) transferrin receptor-targeting (Anti-TfR) liposomes. Liposomes (*red*) and blood vessels (*green*) are shown separately and merged. Scale bar is 20 μm. (b) 3-D renderings of the z-stacks of the images shown in (a), verifying the intravascular location of both liposomes. Images were obtained with a 40 × /1.2 water objective lens.

both types of liposomes were observed in the brain parenchyma (Supplementary Figsure S6 and S7).

DISCUSSION

Even after decades of research, the BBB continues to be a major obstacle in treating several brain disorders (Abbott et al. 2010). Nanomedicine shows potential to enable targeted delivery to the brain by decorating drug-loaded nanoparticles with BBB-targeting ligands, resulting in receptor-mediated uptake and transport across the BBB (Sharma et al. 2019). Here we used liposomes functionalized with OX26, a well-known antibody against the rat TfR, which does not compete with endogenous transferrin (Pardridge 2015). In previous work, the OX26 antibody has shown good specificity toward the rat TfR both *in vitro* and *in vivo*, and liposomes conjugated with the OX26 antibody have shown good targeting ability toward the brain microvasculature in post-natal rats (Johnsen et al. 2017; Thomsen et al. 2019). In the present work, we have combined intravenous injection of Anti-TfR liposomes with FUS-induced increase of BBB permeability to investigate if this approach enhanced the delivery of the Anti-TfR liposomes across the BBB compared with liposomes lacking the targeting moiety.

The liposomes were given 2 h to circulate and attach to the BBB before MBs were injected and FUS was applied. Previous studies have shown good accumulation of TfR-targeted liposomes at the BBB at this time point, and shown comparable amounts of the isotype IgG liposomes and TfR-targeted liposomes still in circulation (Johnsen et al. 2017; Kucharz et al. 2020). US settings used were in the same range as those published by others who achieved safe, local and transient BBBD (McDannold et al. 2008a). In MR images obtained directly after FUS treatment, clear extravasation of the gadolinium contrast agent into the brain parenchyma was observed, showing successful FUS-induced increase of the BBB permeability.

Delivery of the cisplatin-containing liposomes to the brain was quantified by ICP-MS, and the analysis showed a statistically significant increase in brain uptake

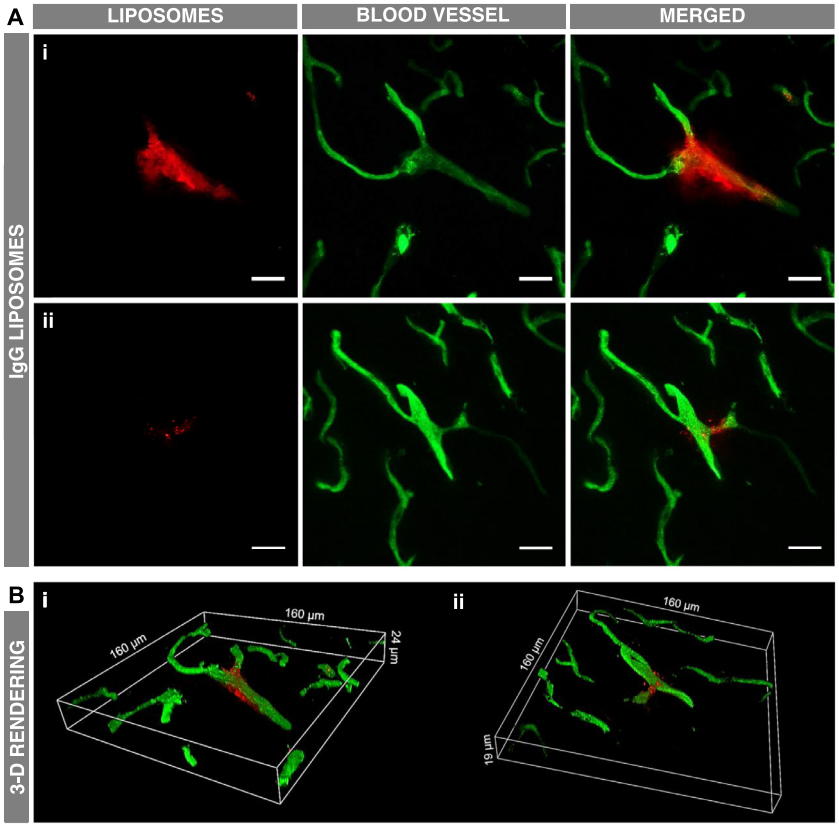

Fig. 6. (a) Representative confocal laser scanning microscopy images acquired in the focused ultrasound-treated hemisphere of animals treated with the isotype immunoglobulin G (IgG) liposome. Liposomes (*red*) and blood vessels (*green*) are shown separately and merged. Liposomes were found to either (i) diffusively stain endothelial cells or (ii) appear as spots aligned with the lectin staining. Scale bar is 20 μm. (b) 3-D renderings of the z-stacks of the images shown in (a), verifying the extravascular location of the liposomes. Images were obtained with a 40 × /1.2 water objective lens.

of the Anti-TfR liposomes in the FUS-treated hemisphere compared with the control hemisphere. Even though a similar degree of BBBD was obtained in animals receiving the IgG liposomes, no increased uptake of the IgG liposomes in the FUS-treated hemisphere was observed.

Possible FUS-induced routes of extravasation are opening of tight junctions, endothelial cell openings (*i.e.,* pore and channel formation), improved endocytosis and increased transcytosis (Sheikov et al. 2004, 2008). While both the isotype IgG and Anti-TfR liposomes might exploit these routes, it is expected that owing to the targeting moiety, the Anti-TfR liposome will benefit mostly from improved endocytosis and transcytosis. FUS-induced increase of clathrin-mediated endocytosis has been reported in different cell types (Hauser et al. 2009; Tardoski et al. 2015; Fekri et al. 2016), which is suggested to most likely be the internalization pathway of TfR-targeting liposomes after receptor binding (Johnsen and Moos 2016). Even though these studies were performed *in vitro*, FUS-induced increase of clathrin-mediated endocytosis could explain the observed increased brain uptake of the Anti-TfR liposomes in the FUS-treated hemisphere compared with the isotype IgG liposomes.

In the control hemisphere, both liposomes accumulated to the same degree. Surprisingly, the Anti-TfR liposome did not perform better than the IgG liposome despite its targeting moiety toward the BBB. Besides the antibody attachment, the lipid composition and physicochemical characteristics of the two liposomes are similar. A possible explanation for this comparable uptake between the isotype IgG and Anti-TfR liposomes might be that IgG liposomes are capable of fusing with the membrane of BCECs, as previously reported (Lindqvist et al. 2016; Hu et al. 2017). Another explanation could be that the 24 h time point was too late to detect any difference between the liposomes. In previous work, no difference in BCEC uptake of the isotype IgG and Anti-TfR liposomes at 24 h was observed, whereas a clear difference was observable at an earlier time point (Johnsen et al. 2017). However, in that study, a clear difference in

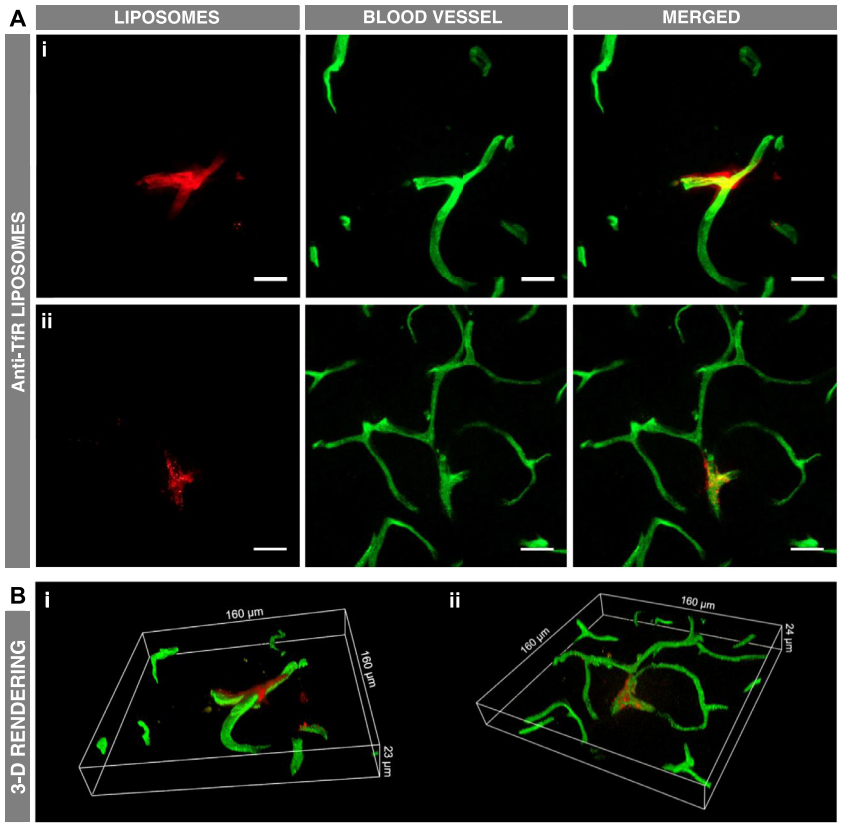

Fig. 7. (a) Representative confocal laser scanning microscopy images acquired in the focused ultrasound-treated hemisphere of animals treated with the transferrin receptor-targeting (Anti-TfR) liposome. Liposomes (*red*) and blood vessels (*green*) are shown separately and merged. Liposomes were found to either (i) diffusively stain endothelial cells or (ii) appear as a spotted structure aligned with the lectin staining. Scale bar is 20 μm. (b) 3-D renderings of the z-stacks of the images shown in (a), verifying the extravascular location of the liposomes. Images were obtained with a 40 $\times$ /1.2 water objective lens.

favor of the Anti-TfR liposomes was still observed in the brain parenchyma after 24 h.

While ICP-MS was performed to quantitatively analyze the effect of FUS treatment on the accumulation of the liposomes, CLSM was performed on brain sections to qualitatively determine the location of the liposomes within the brain tissue. From CLSM tile scans, it was observed that the distribution of liposomes corresponded to gadolinium-enhanced contrast in the MR images (*i.e.,* liposomes accumulated at the location of BBBD). In high-magnification CLSM images acquired in sections of the FUS-treated hemisphere, both liposomes were found to either diffusively stain BCECs or form spots aligned with the lectin staining. Because the displacement of the liposomal fluorescence was only minimal with respect to the lectin staining, it was believed that the observed liposomes were most likely inside the BCECs. Because this kind of staining pattern was not observed for both liposomes in the control hemisphere, it was assumed that the observed accumulation of both the IgG and Anti-TfR liposomes in BCECs was induced by the FUS treatment. The more spotted staining could represent liposomes in intracellular vesicles, and the more diffuse staining could represent intracellular degraded liposomes in the cytoplasm. Both have been observed *in vitro* for Anti-TfR liposomes (Cerletti et al. 2000). Only a small number of both liposomes were observed in the brain parenchyma of the FUS-treated hemisphere, and none in the brain parenchyma of the control hemisphere.

In case of the Anti-TfR liposomes, the mechanism of transferrin receptor-mediated uptake of the liposomes is still not fully understood. Most likely, the TfR-targeted liposomes are endocytosed into clathrin-coated vesicles, similar to the endocytosis of endogenous transferrin complex (Johnsen and Moos 2016). What exactly happens to the TfR-targeted liposomes during the intracellular sorting seems to be affected by the number of antibodies or ligands (Huwyler et al. 1996; Yuan and Zhang 2010) and size and type of the vehicle conjugated to the antibody

(Hatakeyama et al. 2004; Yuan and Zhang 2010). The affinity of the antibody to the TfR will most likely also affect the fate of the TfR-targeted liposomes, but its effect on intracellular sorting and transcytosis has mainly been studied for the use of solely antibodies (Yu et al. 2011; Bien-Ly et al. 2014). Different degrees of brain uptake, intracellular locations of the liposomes and locations of drug release have been observed when these parameters are varied.

Others have hypothesized that drug vehicles decorated with a high-affinity antibody will result in the liposome being transported back into the lumen and intracellularly degraded, with inefficient drug release on the abluminal side (Johnsen and Moos 2016). The OX26 antibody used here is known to have a high affinity toward the transferrin receptor, which could therefore be the reason for the accumulation of the Anti-TfR liposomes in BCECs.

A minimal amount of liposomal fluorescence was observed in the brain parenchyma, which indicates that only a few liposomes were transported into the brain parenchyma by transcytosis or by exploiting the opened tight junctions. However, this does not mean that delivery of cisplatin to the abluminal side was unsuccessful. It has been hypothesized that the cargo of liposomes (*i.e.,* cisplatin) might be released on the abluminal side owing to its endosomal escape during intracellular sorting (Johnsen and Moos 2016). Liposomes that manage to cross the BCEC layer will encounter the basement membrane, which can limit the passage of nanoparticles (Muldoon et al. 1999; Thomsen et al. 2017). The physicochemical characteristics (*e.g.,* charge) of the drug carrier used will most likely determine the successfulness of crossing the basement membrane (Muldoon et al. 1999; Lieleg et al. 2009). After crossing the basement membrane, the liposomes need to distribute through the brain parenchyma by a diffusion-driven process which depends on particle size (Wolak and Thorne 2013; Nance et al. 2014). A drug carrier size of around 100 nm has been suggested to be most efficient in terms of drug delivery across the BBB and diffusion through the brain parenchyma (Gao and Jiang 2006). Diffusion of the relatively large liposome (diameter ~180 nm) used in this study could explain why the liposomal fluorescence was only minimally displaced with respect to the lectin staining.

Even though the exact location of the cisplatin in the brain tissue (*i.e.,* in the endothelial cell or brain parenchyma) is unknown, the increased accumulation demonstrates that FUS and MBs in combination with TfR-targeting liposomes could be a promising approach to enhance drug delivery to the brain.

CONCLUSION

FUS in combination with MBs resulted in an increased delivery of TfR-targeted liposomes to brain tissue, whereas no increased delivery of the isotype IgG liposomes was observed. In the FUS-treated hemisphere, both the isotype IgG and Anti-TfR liposomes were found to mainly associate with BCECs, and only a minimal number of liposomes were found in the brain parenchyma.

Acknowledgments—We thank Torben Moos, Aalborg University, for providing the OX26 antibody and Sofie Snipstad and Sigrid Berg for their technical support with the FUS instrumentation. MRI was performed at the MR Core Facility, Norwegian University of Science and Technology (NTNU). We acknowledge Deborah Hill for her technical assistance with the MRI. Housing of the animals was provided by the Comparative Medicine Core Facility (NTNU). Tissue sections were prepared by the Cellular and Molecular Imaging Core Facility (NTNU). We thank Astrid Bjørkøy and the Centre for Advanced Microscopy at the Faculty of Natural Sciences (NTNU) for technical assistance with CLSM. Illustrations were created with BioRender.com. The project was internally funded by the Norwegian University of Science and Technology and the Technical University of Denmark. Thomas Lars Andresen acknowledges generous support from the Lundbeck Foundation Research Initiative on Brain Barriers and Drug Delivery (www.ribbdd.dk; grant R155-2013-14113).

Conflict of interest disclosure—The authors declare no competing interest.

SUPPLEMENTARY MATERIALS

Supplementary material associated with this article can be found in the online version at doi:10.1016/j.ultrasmedbio.2021.01.014.

REFERENCES

Abbott NJ, Patabendige AA, Dolman DE, Yusof SR, Begley DJ. Structure and function of the blood-brain barrier. Neurobiol Dis 2010;37:13–25.

Alkins R, Burgess A, Ganguly M, Francia G, Kerbel R, Wels WS, Hynynen K. Focused ultrasound delivers targeted immune cells to metastatic brain tumors. Cancer Res 2013;73:1892–1899.

Alonso A, Reinz E, Jenne JW, Fatar M, Schmidt-Glenewinkel H, Hennerici MG, Meairs S. Reorganization of gap junctions after focused ultrasound blood-brain barrier opening in the rat brain. J Cereb Blood Flow Metab 2010;30:1394–1402.

Åslund AK, Berg S, Hak S, Mørch Ý, Torp SH, Sandvig A, Widerøe M, Hansen R, de Lange Davies C. Nanoparticle delivery to the brain—by focused ultrasound and self-assembled nanoparticle-stabilized microbubbles. J Control Release 2015;220:287–294.

Bien-Ly N, Yu YJ, Bumbaca D, Elstrott J, Boswell CA, Zhang Y, Luk W, Lu Y, Dennis MS, Weimer RM, Chung I, Watts RJ. Transferrin receptor (TfR) trafficking determines brain uptake of TfR antibody affinity variants. J Exp Med 2014;211:233–244.

Burgess A, Ayala-Grosso CA, Ganguly M, Jordao JF, Aubert I, Hynynen K. Targeted delivery of neural stem cells to the brain using MRI-guided focused ultrasound to disrupt the blood-brain barrier. PLoS One 2011;6:e27877.

Burgess A, Hynynen K. Noninvasive and targeted drug delivery to the brain using focused ultrasound. ACS Chem Neurosci 2013;4:519–526.

Burgess A, Shah K, Hough O, Hynynen K. Focused ultrasound-mediated drug delivery through the blood-brain barrier. Expert Rev Neurother 2015;15:477–491.

Cerletti A, Drewe J, Fricker G, Eberle AN, Huwyler J. Endocytosis and transcytosis of an immunoliposome-based brain drug delivery system. J Drug Target 2000;8:435–446.

Cho EE, Drazic J, Ganguly M, Stefanovic B, Hynynen K. Two-photon fluorescence microscopy study of cerebrovascular dynamics in ultrasound-induced blood-brain barrier opening. J Cereb Blood Flow Metab 2011;31:1852–1862.

Dhuria SV, Hanson LR, Frey WH, II. Intranasal delivery to the central nervous system: mechanisms and experimental considerations. J Pharm Sci 2010;99:1654–1673.

Etame AB, Diaz RJ, O'Reilly MA, Smith CA, Mainprize TG, Hynynen K, Rutka JT. Enhanced delivery of gold nanoparticles with therapeutic potential into the brain using MRI-guided focused ultrasound. Nanomedicine 2012;8:1133–1142.

Fan CH, Chang EL, Ting CY, Lin YC, Liao EC, Huang CY, Chang YC, Chan HL, Wei KC, Yeh CK. Folate-conjugated gene-carrying microbubbles with focused ultrasound for concurrent blood-brain barrier opening and local gene delivery. Biomaterials 2016;106:46–57.

Fan CH, Ting CY, Chang YC, Wei KC, Liu HL, Yeh CK. Drug-loaded bubbles with matched focused ultrasound excitation for concurrent blood-brain barrier opening and brain-tumor drug delivery. Acta Biomater 2015;15:89–101.

Fan CH, Ting CY, Liu HL, Huang CY, Hsieh HY, Yen TC, Wei KC, Yeh CK. Antiangiogenic-targeting drug-loaded microbubbles combined with focused ultrasound for glioma treatment. Biomaterials 2013;34:2142–2155.

Fekri F, Delos Santos RC, Karshafian R, Antonescu CN. Ultrasound microbubble treatment enhances clathrin-mediated endocytosis and fluid-phase uptake through distinct mechanisms. PLoS One 2016;11 e0156754.

Gao K, Jiang X. Influence of particle size on transport of methotrexate across blood brain barrier by polysorbate 80-coated polybutylcyanoacrylate nanoparticles. Int J Pharm 2006;310:213–219.

Hatakeyama H, Akita H, Maruyama K, Suhara T, Harashima H. Factors governing the in vivo tissue uptake of transferrin-coupled polyethylene glycol liposomes in vivo. Int J Pharm 2004;281:25–33.

Hauser J, Ellisman M, Steinau HU, Stefan E, Dudda M, Hauser M. Ultrasound enhanced endocytotic activity of human fibroblasts. Ultrasound Med Biol 2009;35:2084–2092.

Hu Y, Rip J, Gaillard PJ, de Lange ECM, Hammarlund-Udenaes M. The impact of liposomal formulations on the release and brain delivery of methotrexate: An in vivo microdialysis study. J Pharm Sci 2017;106:2606–2613.

Huwyler J, Wu D, Pardridge WM. Brain drug delivery of small molecules using immunoliposomes. Proc Natl Acad Sci U S A 1996;93:14164–14169.

Hynynen K, McDannold N, Vykhodtseva N, Jolesz FA. Noninvasive MR imaging-guided focal opening of the blood-brain barrier in rabbits. Radiology 2001;220:640–646.

Jefferies WA, Brandon MR, Hunt SV, Williams AF, Gatter KC, Mason DY. Transferrin receptor on endothelium of brain capillaries. Nature 1984;312:162–163.

Johnsen KB, Burkhart A, Melander F, Kempen PJ, Vejlebo JB, Siupka P, Nielsen MS, Andresen TL, Moos T. Targeting transferrin receptors at the blood-brain barrier improves the uptake of immunoliposomes and subsequent cargo transport into the brain parenchyma. Sci Rep 2017;7:10396.

Johnsen KB, Moos T. Revisiting nanoparticle technology for blood-brain barrier transport: Unfolding at the endothelial gate improves the fate of transferrin receptor-targeted liposomes. J Control Release 2016;222:32–46.

Kobus T, Zervantonakis IK, Zhang Y, McDannold NJ. Growth inhibition in a brain metastasis model by antibody delivery using focused ultrasound-mediated blood-brain barrier disruption. J Control Release 2016;238:281–288.

Kucharz K, Kristensen K, Johnsen KB, Lund MA, Lønstrup M, Moos T, Andresen TL, Lauritzen MJ. Post-capillary venules is the locus for transcytosis of therapeutic nanoparticles to the brain. bioRxiv 2020; 2020.06.05.133819.

Lieleg O, Baumgartel RM, Bausch AR. Selective filtering of particles by the extracellular matrix: an electrostatic bandpass. Biophys J 2009;97:1569–1577.

Lindqvist A, Friden M, Hammarlund-Udenaes M. Pharmacokinetic considerations of nanodelivery to the brain: Using modeling and simulations to predict the outcome of liposomal formulations. Eur J Pharm Sci 2016;92:173–182.

Liu HL, Fan CH, Ting CY, Yeh CK. Combining microbubbles and ultrasound for drug delivery to brain tumors: current progress and overview. Theranostics 2014;4:432–444.

Liu HL, Hua MY, Chen PY, Chu PC, Pan CH, Yang HW, Huang CY, Wang JJ, Yen TC, Wei KC. Blood-brain barrier disruption with focused ultrasound enhances delivery of chemotherapeutic drugs for glioblastoma treatment. Radiology 2010;255:415–425.

Lochhead JJ, Thorne RG. Intranasal delivery of biologics to the central nervous system. Adv Drug Deliv Rev 2012;64:614–628.

McDannold N, Vykhodtseva N, Hynynen K. Blood-brain barrier disruption induced by focused ultrasound and circulating preformed microbubbles appears to be characterized by the mechanical index. Ultrasound Med Biol 2008a;34:834–840.

McDannold N, Vykhodtseva N, Hynynen K. Effects of acoustic parameters and ultrasound contrast agent dose on focused-ultrasound induced blood-brain barrier disruption. Ultrasound Med Biol 2008b;34:930–937.

Meairs S, Alonso A. Ultrasound, microbubbles and the blood-brain barrier. Prog Biophys Mol Biol 2007;93:354–3662.

Moos T, Oates PS, Morgan EH. Expression of the neuronal transferrin receptor is age dependent and susceptible to iron deficiency. J Comp Neurol 1998;398:420–430.

Muldoon LL, Pagel MA, Kroll RA, Roman-Goldstein S, Jones RS, Neuwelt EA. A physiological barrier distal to the anatomic blood-brain barrier in a model of transvascular delivery. AJNR Am J Neuroradiol 1999;20:217–222.

Mullin L, Gessner R, Kwan J, Kaya M, Borden MA, Dayton PA. Effect of anesthesia carrier gas on in vivo circulation times of ultrasound microbubble contrast agents in rats. Contrast Media Mol Imaging 2011;6:126–131.

Nance E, Timbie K, Miller GW, Song J, Louttit C, Klibanov AL, Shih TY, Swaminathan G, Tamargo RJ, Woodworth GF, Hanes J, Price RJ. Non-invasive delivery of stealth, brain-penetrating nanoparticles across the blood-brain barrier using MRI-guided focused ultrasound. J Control Release 2014;189:123–132.

Nhan T, Burgess A, Cho EE, Stefanovic B, Lilge L, Hynynen K. Drug delivery to the brain by focused ultrasound induced blood-brain barrier disruption: Quantitative evaluation of enhanced permeability of cerebral vasculature using two-photon microscopy. J Control Release 2013;172:274–280.

Pardridge WM. Drug transport across the blood-brain barrier. J Cereb Blood Flow Metab 2012;32:1959–1972.

Pardridge WM. Blood-brain barrier drug delivery of IgG fusion proteins with a transferrin receptor monoclonal antibody. Expert Opin Drug Deliv 2015;12:207–222.

Poon C, McMahon D, Hynynen K. Noninvasive and targeted delivery of therapeutics to the brain using focused ultrasound. Neuropharmacology 2017;120:20–37.

Rapoport SI. Osmotic opening of the blood-brain barrier: Principles, mechanism, and therapeutic applications. Cell Mol Neurobiol 2000;20:217–230.

Sharma G, Sharma AR, Lee SS, Bhattacharya M, Nam JS, Chakraborty C. Advances in nanocarriers enabled brain targeted drug delivery across blood brain barrier. Int J Pharm 2019;559:360–372.

Sheikov N, McDannold N, Sharma S, Hynynen K. Effect of focused ultrasound applied with an ultrasound contrast agent on the tight junctional integrity of the brain microvascular endothelium. Ultrasound Med Biol 2008;34:1093–1104.

Sheikov N, McDannold N, Vykhodtseva N, Jolesz F, Hynynen K. Cellular mechanisms of the blood-brain barrier opening induced by ultrasound in presence of microbubbles. Ultrasound Med Biol 2004;30:979–989.

Tardoski S, Gineyts E, Ngo J, Kocot A, Clezardin P, Melodelima D. Low-intensity ultrasound promotes clathrin-dependent endocytosis

for drug penetration into tumor cells. Ultrasound Med Biol 2015;41:2740–2754.

Taylor EM, Morgan EH. Developmental changes in transferrin and iron uptake by the brain in the rat. Brain Res Dev Brain Res 1990;55:35–42.

Thomsen LB, Linemann T, Birkelund S, Tarp GA, Moos T. Evaluation of targeted delivery to the brain using magnetic immunoliposomes and magnetic force. Materials (Basel) 2019;12:3576.

Thomsen MS, Routhe LJ, Moos T. The vascular basement membrane in the healthy and pathological brain. J Cereb Blood Flow Metab 2017;37:3300–3317.

Ting CY, Fan CH, Liu HL, Huang CY, Hsieh HY, Yen TC, Wei KC, Yeh CK. Concurrent blood-brain barrier opening and local drug delivery using drug-carrying microbubbles and focused ultrasound for brain glioma treatment. Biomaterials 2012;33:704–712.

Treat LH, McDannold N, Zhang Y, Vykhodtseva N, Hynynen K. Improved anti-tumor effect of liposomal doxorubicin after targeted blood-brain barrier disruption by MRI-guided focused ultrasound in rat glioma. Ultrasound Med Biol 2012;38:1716–1725.

White E, Woolley M, Bienemann A, Johnson DE, Wyatt M, Murray G, Taylor H, Gill SS. A robust MRI-compatible system to facilitate highly accurate stereotactic administration of therapeutic agents to targets within the brain of a large animal model. J Neurosci Methods 2011;195:78–87.

Wolak DJ, Thorne RG. Diffusion of macromolecules in the brain: implications for drug delivery. Mol Pharm 2013;10:1492–1504.

Yu YJ, Zhang Y, Kenrick M, Hoyte K, Luk W, Lu Y, Atwal J, Elliott JM, Prabhu S, Watts RJ, Dennis MS. Boosting brain uptake of a therapeutic antibody by reducing its affinity for a transcytosis target. Sci Transl Med 2011;3 84ra44.

Yuan HY, Zhang SL. Effects of particle size and ligand density on the kinetics of receptor-mediated endocytosis of nanoparticles. Appl Phys Lett 2010;96 033704.